International Journal of Engineering Research and Technology. ISSN 0974-3154, Volume 12, Number 9 (2019), pp. 1538-1543

Determination of geometric factor for crack growing from a notch

Oscar Araque[1*], Eduardo Perez[2], Luis Fabian Urrego[3] and Laura Gallego[4]

[1,2,3] *Programa de Ingeniería Mecánica, Universidad de Ibagué, Ibagué, Colombia*

[1*]*ORCID: 0000-0001-9400-1140* [2]*ORCID: 0000-0002-9983-5926*

[4]*Programa de Contaduría Pública, Universidad Cooperativa de Colombia, Ibagué – Espinal, Colombia.*

[4]*ORCID: 0000-0003-3131-235X*

Abstract

This manuscript studies the behavior of an ASTM A 36 structural steel specimen with a circular stress concentrator of variable diameter and a notch using computational modeling of finite elements (Ansys) and fracture mechanics, the test specimen has a thickness of 5 mm and a notch of 30 mm with opening of 45° was subjected to cyclic axial load and the diameter of the concentrator varies from 5mm, 9mm, 13mm, 17mm and 21 mm. This in order to establish the function that describes the behavior of the dimensionless geometrical factor (β) in the calculation of the Stress Intensity Factor (SIF). For each selected diameter, the characteristic equation is obtained using the Support Vector Machine algorithm based on the Kernel equations. These results were compared with other accepted modes, obtaining a high degree of correlation and an error percentage close to 1.7%. As a main contribution, a new general mathematical model is obtained for specimens of defined geometry and concentrator of circular stress.

Keywords: Stress Intensity Factor, geometric factor, crack growth, ANSYS, structural steel, regression, Kernels.

I. INTRODUCTION

Fracture toughness is a mechanical property that measures the ability to resist stress before fracture, this science originates from the fundamental works proposed by Griffith (1921, 1924), the researcher Irwin (1957) makes an important advance by proposing the analysis of fracture toughness in terms of tensions, Stress intensity factor (SIF) of a material is a function of the applied stress, and the length of the crack, but given the different configurations to perform the tests, these values are known as a function of the failure modes called Stress Instensity Factor SIF K1(Opening), K2 (in plane shear) y K3 (out of plane shear).

The determination of the Stress intensity factor in materials with linear elastic behavior (LEFM) is possible using the quantification of the stresses around the crack tip as a function of the nominal stress and the crack size used. The Finite Element Analysis (FEM) method allows testing in virtually any of the configurations described above due to the ease of imposing the variables, if there a component of analysis for the propagation of crack Extended finite element method (XFEM), it is possible to perform simulations in order to verify the behavior of the geometric factor that accompanies the estimation of fracture toughness in the different modes of failure, recently author Nairn [1], proposed to analyze the geometric factor as a correction factor of the general equation of toughness, and that this same one, can be expressed in function of the length of crack (a) and in function of the width (w), on the other hand, according to the author Mecholsky, the geometric factor (Y) for semi-elliptic cracks in materials with high hardness and brittleness explains the position and shape of the crack since it is a function of an angle (θ) between the surface of the crack front and any peripheral point on it [2]. However, the authors Taylor, Cornetti and Pugno, catalogued this geometric factor, not only as a function of geometry, but also as a function of the crack notch [3].

On the other hand, when analyzing the propagation of cracks to fatigue, the geometrical factor is involved within an expression known as the initial propagation value for short cracks (a0), which according to the authors Atzori, Lazzarin and Meneghetti, appears at the intersection place between the change of the stress (Δσ) and the different tenacity values (ΔK), where the geometrical factor is calculated using a simulation in the ANSYS 5.6 software. [4], Similarly, when analyzing ceramic materials, the authors Smith and Scattergood define toughness as a sum of two different toughnesses, the first (Kbend) is a toughness that is a function of the Stress intensity factor for a deflection stress curve, and the second a residual toughness (Kresidual) that results from the field of residual stresses due to stress, then it is stated that the value of tenacity (Kbend) is affected by a form factor (H) which is a function of (a) which is the depth of the crack and (c) which is the length of the crack, this approximation is described by an equation of exponential nature, where the base is the relation (a⁄c) [5]. However, when materials with a higher degree of ductility are analyzed, the empirical approximations made by authors Newman and Raju show an exponential behavior for the form factor (Q), whose base is the ratio (a⁄c), where (a) is the depth of the crack and (c) is the length of the crack, this approximation is valid for when the ratio (a⁄c) is less than or equal to the unit [6], on the other hand, when testing chromium steels, authors Nix and Lindley determined that the behavior of the form factor (Cs) was also exponential in nature, where the basis was again the relationship (a⁄c), where (a) is the depth of the crack, and (c) is the length of the crack, the values of this ratio were previously calculated, subjecting specimens of chromium steel with small cracks to frictional forces, the results showed that for that configuration, the values of the ratio

(a⁄c) are less than 1, and that the best corrections to the fracture toughness equation were achieved with values less than 0.2, in the same way, this form factor would be computed with a second factor they defined as (Mf) which is a correction factor in the crack front, which is also of an exponential nature and is a function of the relationship (a⁄c) [7], these correction factors have been the product of a rigorous analytical analysis, where the foundation of each of the equations that describe these factors, starts from simulations in finite element programs, which provide the input values necessary to apply the respective analysis algorithms, as proposed by the authors Clarke, Griebsch and Simpson, who explain how it is possible to glimpse different situations of a mechanical nature by means of the Support Vector Regression (SVR) algorithm, this algorithm allows from some input values in the Cartesian plane, to obtain an equation that fits the distribution of values given, considering the dispersion (ξ) of the same, and the margin (ε) between the support vectors [8]. This algorithm uses Lagrange optimization principles, simultaneously involving Kernel functions, which can be polynomial, Gaussian or Sigmoidal, as explained by authors Schölkopf and Smola [9], authors Heydari and Choupani, describe a correction factor for fracture toughness of logarithmic nature based on energy release rate [10], authors El-Desouky and El-Wazery, defined fracture toughness for materials with high degree of fragility, using a polynomial of fifth degree (F1), whose variable is the relationship (a⁄w) [11].

II. MATERIALS AND PROCEDURE

Algorithm Support Vector Regression. The SVR algorithm is an algorithm developed in Russia during the 1960s, by Vapnik [12], which consists of generating an interpolation equation from vectors directed at points in the plane, taking into account variance (σ) and dispersion (ζ), using equations that describe different behaviors in space called Kernel equations. Several of these equations appear in Table 1.

Table 1. Common Kernel Equations [13]

Lineal	$k(x) = (\gamma * x + \varphi)$
Polynomial	$k(x) = (\gamma * x + \varphi)^d$
Gaussian	$k(x) = e^{\gamma * (x-\mu)^2}$
Sigmoidal	$k(x) = \tanh(\gamma * x + \varphi)$

Based on the Kernel equations a unitary matrix is formed in the diagonal, from which, by means of a quadratic optimization the Lagrange multipliers $(\propto_i^* - \propto_i)$ will be found according to the approach (1).

$$Maximize \begin{cases} -\frac{1}{2}\sum_{i=1}^{\ell}(\propto_i^* - \propto_i)(\propto_j^* - \propto_j)k(x) \\ -\varepsilon\sum_{i=1}^{\ell}(\propto_i^* - \propto_i) + \sum_{i=1}^{\ell} y_i(\propto_i^* - \propto_i) \end{cases} \quad (1)$$

$$subjet\ to \begin{cases} \sum_{i=1}^{\ell}(\propto_i^* - \propto_i) = 0 \\ \alpha_i \alpha_i^* \in [0, C] \end{cases} \quad (2)$$

Then the complete approximation is given by the expression (3)

$$f(x) = \sum_{i=1}^{\ell}(\propto_i^* - \propto_i) * k(x) + b \quad (3)$$

Simulation Finite Element Method. The purpose of the research article is to determine the behavior of the geometric factor, as an element of correction of the general equation of stress intensity factor (SIF); for the fundamental conception of the work, five test specimen were used, which were modeled using the finite element software ANSYS 19.2 and analysis by Smart Crack Growth, the values of crack length (a) are obtained for each iteration made during the simulation with the value of SIF, having previously defined the material as structural steel ASTM A-36, the characteristics of the material are indicated in Table 2.

Table 2. Mechanical properties of steel ASTM A36 [14]

Mechanical Properties	Magnitude
Tensile Strength Yield	250 MPa
Tensile Strength Ultimate	400-550 MPa
Modulus of Elasticity	200 GPa
Poisson's Ratio	0,26
Shear Modulus	79,3 GPa

The specimen has a thickness of 5 mm and a notch of 30 mm with opening of 45°, Figure 1 shows the geometry of the specimen and Figure 2 shows the test specimen used in Ansys 19.2.

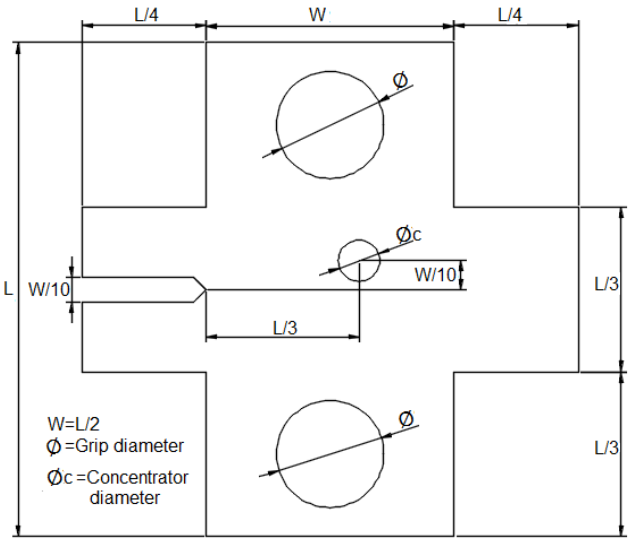

(a)

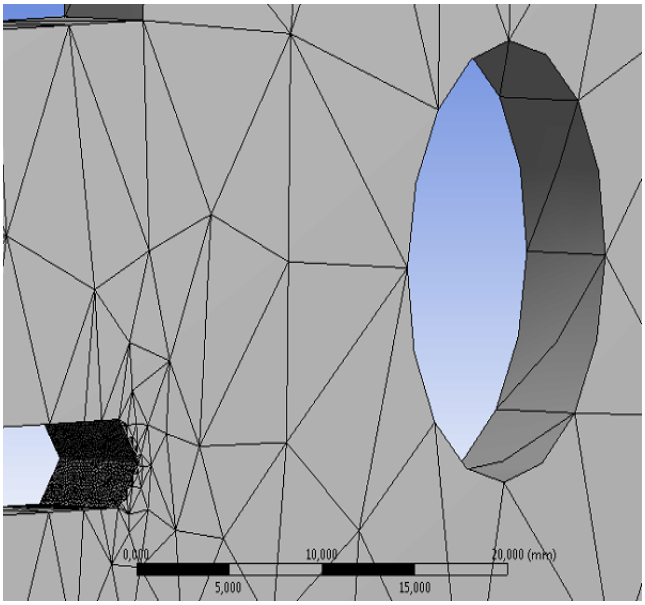

(b)

Fig. 1. (a) Dimensions for the specimen used, (b) mesh notch doing for the FE analysis

Computational Model. The optimal computational model for the processing of the values of (K_1) and their respective values of (a) was chosen considering the processing load and the affinity of the results, thus, the computational model was proposed, proposing a type of bonded contact in the connections of the elements, for the refinement of the mesh the Edge Sizing method was introduced, together with a Patch Conforming method with a tetrahedric definition, in the same way, the Pre-Meshed Crack method was involved within the Fracture component, the Pre-Meshed Crack method which involves the crack front that is used by the Smart Crack Growth analysis engine where the failure criterion is SIF with a value of 131.6 $MPa\sqrt{m}$ for structural steel ASTM A36, determined by E. Ghafoori and M. Motavalli on an experimental basis [15].

Numerical Model. The most suitable numerical model of finite elements for computational processing is selected, referring to Stress intensity factor mode 1 (KI), three numerical models were formulated and the relative error for each of these models was determined from the theoretical value of K_I estimated according to [16,17, 18]. As shown in Table 3.

Table 3. CPU Performance Vs. Relative Error

	Nodes	Elements	CPU Time (min)	KI (Pa sqrt(m))	% Error
Analytical Model of Anderson				4.75e12	
Numerical Model 1	86070	47340	1h 52 m	4.80e12	1.5
Numerical Model 2	48870	25240	1h 2m	4.38e13	4.2

It can be observed that numerical model 1 presents an adequate balance between computational cost and error percentage.

Calculation of Geometric Factor Values. For the calculation of the values of the geometrical factor, the equation of the Stress intensity factor (SIF) was considered, where a geometrical factor was involved (β), which is cleared from the expression (3), since the values for (K_I) the crack length (a) are obtained for each iteration.

$$K_I = \beta\sigma\sqrt{\pi a} \quad (4)$$

Where (σ) is the nominal applied stress and (a) is the length of the crack, clearing (β) of the expression (3), is obtained (4).

$$\beta = \frac{K_I}{\sigma\sqrt{\pi a}} \quad (5)$$

Ratio Calculation (a/w). The relation (a /w) (5) is a proportion between the length of the crack and the width of the face where the nominal stress acts (σ), a third variable (r) was involved which is the radius of the stress concentrator present in the geometry of the specimen, this concentrator is included for the purpose of verifying the behavior of propagation when there is a variable radius stress concentrator.

$$\frac{a}{w} \quad (7)$$

III. RESULTS

From the simulation in ANSYS 19.2 K_I and (a) values were generated for each iteration, using equation (4) and (5), Figure 3 is constructed for a 5 mm diameter concentrator:

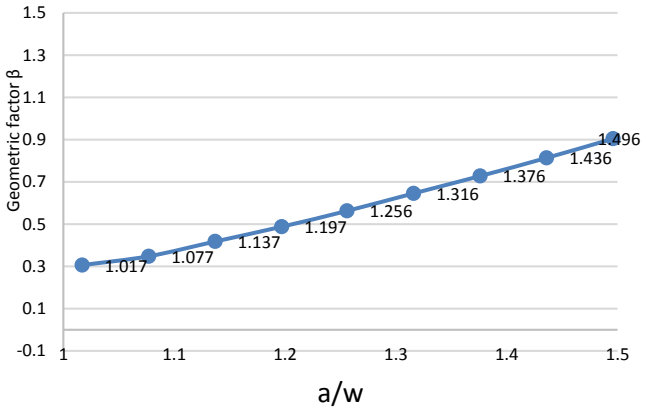

Fig. 2. Entry points to the SVR for 5 mm diameter concentrator.

Once the entry points are obtained, one of the Kernel equations is chosen, whose behavior is similar to that shown in figure 3. It was determined that the Gaussian model adapts well, equation (8).

$$k(x) = e^{\gamma*(x-\mu)^2} \quad (8)$$

Based on this function the Kernel matrix is formed, 9 points were used for the input values to the SVR model, the variance (σ) has been estimated as 0.181

$$K = \begin{bmatrix} 1.00 & 0.94 & 0.93 & 0.94 & 0.92 & 0.94 & 0.94 & 0.94 & 0.94 \\ 0.94 & 1.00 & 0.94 & 0.93 & 0.94 & 0.92 & 0.94 & 0.94 & 0.94 \\ 0.93 & 0.94 & 1.00 & 0.94 & 0.93 & 0.94 & 0.92 & 0.94 & 0.94 \\ 0.94 & 0.93 & 0.94 & 1.00 & 0.94 & 0.93 & 0.94 & 0.92 & 0.94 \\ 0.92 & 0.94 & 0.93 & 0.94 & 1.00 & 0.94 & 0.93 & 0.94 & 0.92 \\ 0.94 & 0.92 & 0.94 & 0.93 & 0.94 & 1.00 & 0.94 & 0.93 & 0.94 \\ 0.94 & 0.94 & 0.92 & 0.94 & 0.93 & 0.94 & 1.00 & 0.94 & 0.93 \\ 0.94 & 0.94 & 0.94 & 0.92 & 0.94 & 0.93 & 0.94 & 1.00 & 0.94 \\ 0.94 & 0.94 & 0.94 & 0.94 & 0.92 & 0.94 & 0.93 & 0.94 & 1.00 \end{bmatrix}$$

The Lagrange multipliers are obtained from the Kernel matrix by means of optimization under square conditions. With Lagrange multipliers, the expression of the SVR algorithm (8) is used to obtain the F(x) shown in (9) function that interpolates the entry points.

$$\sum_{i=1}^{\ell}(\propto_i^* - \propto_i) * K(x) + b$$

In this way, we proceed to add the multipliers of Lagrange obtained to find the coefficient that accompanies the Kernel function selected in (6).

$$f(x) = 0.01 * e^{\frac{x^2}{2\sigma^2}} + 0.3 \qquad (9)$$

The resulting equations for each modeled specimen are shown in Table 4, for parameterization reasons, it is called $\left(x = \frac{a}{w}\right)$

Table 4. Equations for each specimen

Specimen	$\emptyset_c$(cm)	Equation
1	0.5	$\beta = 7.10\text{x}10^{-15} * e^{\frac{\left(\frac{a}{w}\right)^2}{7.22}}$
2	0.9	$\beta = 0.275 * e^{\frac{\left(\frac{a}{w}\right)^2}{1.92}}$
3	1.3	$\beta = 1 * e^{\frac{\left(\frac{a}{w}\right)^2}{0.76}}$
4	1.7	$\beta = 7.47x10^{-16} * e^{\frac{\left(\frac{a}{w}\right)^2}{0.045}}$
5	2.0	$\beta = 3.55x10^{-15} * e^{\frac{\left(\frac{a}{w}\right)^2}{0.79}}$

From these equations, it was possible to obtain a mathematical expression that links all the previous expressions, this expression was obtained by integrating each of the equations of Table 4. And adding the areas under the curve of each of them, obtaining the general expression (10).

$$\beta = \mathbf{7.05x10^{-14}} * \boldsymbol{e}^{\mathbf{0.13}*\left(\frac{\boldsymbol{a}}{\boldsymbol{w}}\right)^2} + \mathbf{0.26} * \boldsymbol{e}^{\mathbf{0.51}*\left(\frac{\boldsymbol{a}}{\boldsymbol{w}}\right)^2} + \mathbf{1} * \boldsymbol{e}^{\mathbf{1.30}*\left(\frac{\boldsymbol{a}}{\boldsymbol{w}}\right)^2} + \mathbf{7.51x10^{-16}} * \boldsymbol{e}^{\mathbf{22.65}*\left(\frac{\boldsymbol{a}}{\boldsymbol{w}}\right)^2} + \mathbf{3.52x10^{-15}} * \boldsymbol{e}^{\mathbf{1.25}*\left(\frac{\boldsymbol{a}}{\boldsymbol{w}}\right)^2} \qquad (10)$$

In equation (10), if (a/w) assumes very small values, the mathematical expressions calculated for specimens 1, 4 and 5 tend to 0, therefore the general expression is as shown in (11):

$$\beta = f(a/w) = \mathbf{0.26} * \boldsymbol{e}^{\mathbf{0.51}*\left(\frac{\boldsymbol{a}}{\boldsymbol{w}}\right)^2} + \boldsymbol{e}^{\mathbf{1.30}*\left(\frac{\boldsymbol{a}}{\boldsymbol{w}}\right)^2} \qquad (11)$$

The researcher Anderson [16], raises five mathematical models for the function f(a⁄w) finding the following ones: Single-edge notched tension (SENT), Singled-edge notched bend (SE(B)), Center cracked tension (CCT), Double-edge notched tension (DENT) and Compact Specimen (CP), each of these is preceded by a term that adjusts the function, in the proposed model, that term will be the second derivative of the function $f(a/w)$, so that the corrected model remains as indicated in (12).

$$\beta = \boldsymbol{\Omega} * f(a/w) \qquad (12)$$

Where Ω is the second derivate of the function $f(a/w)$, obtaining the model of equation (13).

$$\beta = \frac{\boldsymbol{d^2} f(a/w)}{\boldsymbol{d} f(a/w)^{\mathbf{2}}} * f(a/w) \qquad (13)$$

The adjusted model (14) is obtained by operating the functions.

$$\boldsymbol{\beta} = \left[\mathbf{2.6} * \mathbf{e}^{\mathbf{1.3}*\left(\frac{\mathbf{a}}{\mathbf{w}}\right)^2} + \mathbf{0.26} * \mathbf{e}^{\mathbf{0.51}*\left(\frac{\mathbf{a}}{\mathbf{w}}\right)^2} + \mathbf{0.27} * \left(\frac{\mathbf{a}}{\mathbf{w}}\right)^2 * \mathbf{e}^{\mathbf{0.51}*\left(\frac{\mathbf{a}}{\mathbf{w}}\right)^2} + \mathbf{6.76} * \left(\frac{\mathbf{a}}{\mathbf{w}}\right)^2 * \mathbf{e}^{\mathbf{1.30}*\left(\frac{\mathbf{a}}{\mathbf{w}}\right)^2}\right] * \left[\mathbf{e}^{\mathbf{1.3}*\left(\frac{\mathbf{a}}{\mathbf{w}}\right)^2} + \mathbf{0.26} * \mathbf{e}^{\mathbf{0.51}*\left(\frac{\mathbf{a}}{\mathbf{w}}\right)^2}\right] \qquad (14)$$

Fig. 3 shows the Proposed Model graph for $0 < a/w < 1$. From (12) the maximum absolute error (MAE), the average absolute error (AAE) and the root mean square error (RMSE) are calculated using the coordinates y of each point used in the SVR algorithm. The equations used to calculate each of these parameters between the values obtained for the proposed model (PM) and the compact model (CP) enunciated by [16] are shown in Table 5.

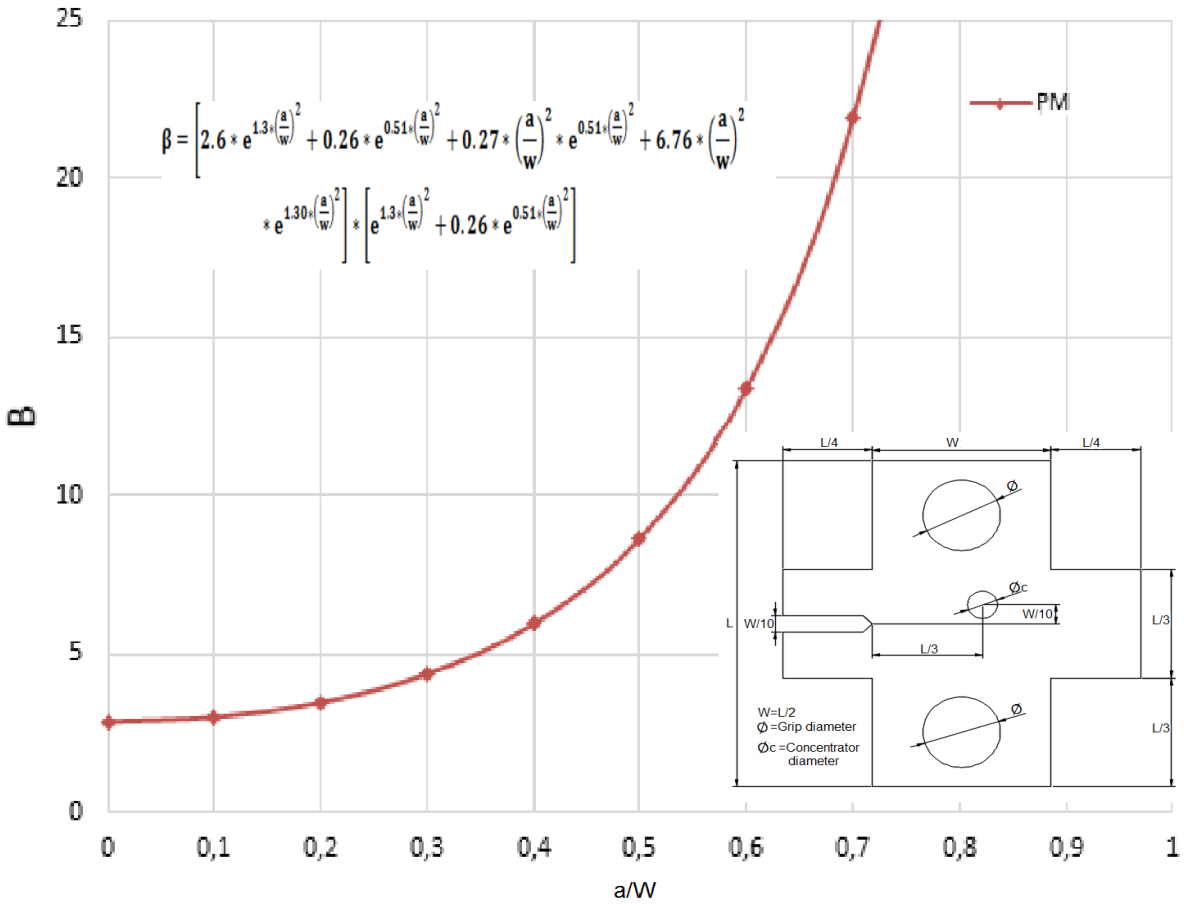

Fig. 3. Graph of the proposed model (PM)

Table 5. Error measures for accuracy assessment between the PM and CP [17]

Name	equation	Error (%)
Max. Absolute Error (MAE)	$Max.\|y_i - y_i^*\| \dots i = 1,..,n_{error}$	6.3
Average Absolute Error (AAE)	$\frac{1}{n_{error}} * \sum_{i=1}^{n_{error}} \|y_i - y_i^*\|$	0.63
Root Mean Square Error (RMSE)	$\sqrt{\frac{\sum_{i=1}^{n_{error}} \|y_i - y_i^*\|^2}{n_{error}}}$	1.7

Implementing better valuation methods can reduce the costs associated with repairs for damage associated with material failures [19].

IV. CONCLUSION

The Support Vector Machine SVM algorithm is used for the purpose of establishing the characteristic equation of the dimensionless geometric factor used for the determination of Stress intensity factor in a test specimen subjected to axial load. This algorithm is based on the application of the Kernel equations, applying the Lagrange square optimization principle.

The modeling of a structural steel ASTM A 36 specimen with thickness of 5 mm and a notch of 30 mm with opening of 45° was carried out. A circular stress concentrator with variable diameter of 5mm, 9mm, 13mm, 17mm and 21 mm is applied to this specimen, obtaining the function that describes the behaviour of the dimensionless factor for each one of the selected diameters.

From the equations obtained by the SVR model, these are compared with the computational model, obtaining a Max. Absolute Error (MAE) of 6.3%, the Average Absolute Error (AAE) of 0.63% and Root Mean Square Error (RMSE) de 1.7%, which is a good indication of the approximation obtained, with reference to a similar model.

With the data compiled for the simulated specimens, it was possible to obtain a generalized equation for the dimensionless geometrical factor (β), which involves the relationship between the size of the crack (a) and the width of the transversal section of the analyzed specimen (W). This equation defines the generalized dimensionless variable for specimens subjected to axial load with a circular geometry concentrator.

ACKNOWLEDGMENTS

The authors would like to thank the Research Department at the Universidad de Ibagué and the Universidad Cooperativa de Colombia for their support provided for the development of this research.

REFERENCES

[1] Nairn, J.A., "Direct comparison of anisotropic damage mechanics to fracture mechanics of explicit cracks", *Engineering Fracture Mechanics*, No. 203, (2018), 197-207.

[2] Mecholsky Jr, J., "Fracture mechanics principles", *Dental Materials*, Vol. 11, No. 2, (1995), 111-112.

[3] Taylor, D., Cornetti, P., & Pugno, N., "The fracture mechanics of finite crack extension", *Engineering Fracture Mechanics*, Vol. *72*, No. 7, (2005), 1021-1038.

[4] Atzori, B., Lazzarin, P., & Meneghetti, G., "Fracture mechanics and notch sensitivity", *Fatigue & Fracture of Engineering Materials & Structures*, Vol. 26, No. 3, (2003), 257-267.

[5] Smith, S. M., & Scattergood, R. O., "Crack-shape effects for indentation fracture toughness measurements", *Journal of the American Ceramic Society*, Vol. 75, No. 2, (1992), 305-315.

[6] Newman Jr, J. C., & Raju, I. S., "An empirical stress-intensity factor equation for the surface crack", *Engineering fracture mechanics*, Vol. 15, No. (1-2), (1981), 185-192.

[7] Nix, K. J., & Lindley, T. C., "The application of fracture mechanics to fretting fatigue", *Fatigue & Fracture of Engineering Materials & Structures*, Vol. 8, No. 2, (1985), 143-160.

[8] Clarke, S. M., Griebsch, J. H., & Simpson, T. W., "Analysis of support vector regression for approximation of complex engineering analyses", *Journal of mechanical design*, Vol. 127, No. 6, (2005), 1077-1087.

[9] Smola, A. J., & Schölkopf, B., "A tutorial on support vector regression", *Statistics and computing*, Vol. 14, No. 3, (2004), 199-222.

[10] Heydari, M. H., & Choupani, N., "A new comparative method to evaluate the fracture properties of laminated composite", *International Journal of Engineering*, Vol. 27, No. 6, (2014), 1025-2495.

[11] EL-Desouky, A. R., & El-Wazery, M. S., "Mixed mode crack propagation of zirconia/nickel functionally graded materials", *International Journal of Engineering (IJE)*, Vol. 26, No. 8, (2013), 885-894.

[12] Vapnik, V., "The Nature of Statistical Learning Theory", Springer, New York, (1995).

[13] Clarke, S. M., Griebsch, J. H., & Simpson, T. W., "Analysis of support vector regression for approximation of complex engineering analyses", *Journal of mechanical design*, Vol. 127, No. 6, (2005), 1077-1087.

[14] MatWeb, L. L. C. Material property data. MatWeb,[Online]. Available: http://www. matweb. com. (2019).

[15] Ghafoori, E., Motavalli, M., Botsis, J., Herwig, A., & Galli, M., "Fatigue strengthening of damaged metallic beams using prestressed unbonded and bonded CFRP plates", *International Journal of Fatigue*, No. 44, (2012), 303-315.

[16] Anderson, T. L., "Fracture mechanics: fundamentals and applications", CRC press, (2017).

[17] Araque, O., Arzola, N., & Varón, O., "Computational modeling of fatigue crack propagation in butt welded joints subjected to axial load", *PloS one*, Vol. 14, No. 6, (2019), 1-17.

[18] Hernández Laguna, E., Arzola de la Peña, N., & Araque de los Ríos, O., Fracture mechanics assessment of fatigue semi-elliptical cracks in butt-welded joints. Ingeniare. Revista chilena de ingeniería, Vol. 26, Nº 4, (2018), 568-576.

[19] Gallego Cossio, L., & Hernandez Aros, L., "Methods of Economic-Financial Valuation: Analysis from a Case of Study", International Business Management, Vol. 12, Nº 2, (2018), 196-204.